Evidence of charge delocalization in $Ce_{1-x}Fe_x^{2+(3+)}O_{2-y}$ nanocrystals ($x = 0, 0.06, 0.12$)

Z. V. Popović, Z. D. Dohčević-Mitrović, N. Paunović, and M. Radović

Center for Solid State Physics and New Materials, Institute of Physics, University of Belgrade, Pregrevica 118, 11080 Belgrade, Serbia

(Received 28 January 2011; revised manuscript received 15 November 2011; published 18 January 2012)

We have measured Raman scattering spectra of pure and iron-doped $Ce_{1-x}Fe_x^{2+(3+)}O_{2-y}$ ($x = 0$, 0.06, and 0.12) nanocrystals. According to the x-ray diffraction study, Fe doping produces contraction of the CeO_2 unit cell, leading to the Raman mode hardening. Contrary to expectation, the F_{2g} Raman mode exhibits softening and broadening by changing the valence state of Fe dopant, as a consequence of the electron-molecular vibration coupling. This finding supports the assumption that additional charge in highly oxygen-deficient pure and Fe-doped CeO_{2-y} samples are not only localized at Ce^{3+} ions but also delocalized onto Ce(Fe)-O(V_O)-Ce(Fe) orbitals. Delocalization of electrons from Ce^{3+} ions causes insulator-to-metal transition in highly oxygen-deficient nanoceria. The far-infrared reflectivity spectrum of nanoceria shows metalliclike reflectivity, which in the low-frequency region is well fitted with the Hagen-Rubens approximation for metals. Photoluminescence measurements revealed the existence of a defect-related band in the energy gap of CeO_{2-y}. The electron-molecular vibration (phonon) coupling constants λ and density of electron states at the Fermi level per spin and molecule $N(0)$ were determined within the framework of Allen's theory. The proposal of an energy band structure of nanoceria is also presented.

DOI: 10.1103/PhysRevB.85.014302 PACS number(s): 78.30.Hv, 78.55.Hx, 63.20.kd, 63.22.Kn

I. INTRODUCTION

Ultrafine ceria powders represent an important material for solid oxide fuel cells or catalytic applications, which are attributed to the remarkable oxygen-storage capability of CeO_2, i.e., the ability to undergo rapid redox cycles by releasing and storing oxygen. Oxygen vacancies often play a crucial rule in changing material properties.[1,2] According to many electronic structure calculations[3–7] of CeO_{2-y}, based on the density-functional theory with the Hubbard U parameter correction (DFT+U formalism), the formation of vacancies in CeO_2, in the standard picture of charge localization, is accompanied by localization of two electrons on the f level of two neighboring Ce ions. The value of $U = 6$ eV, which represents the strong on-site Coulomb repulsion among the localized Ce $4f$ electrons, is obtained to reproduce a certain set of experimental data as band gaps or crystal lattice parameters. Very recent DFT+U calculations show that the charge prefers to distribute itself so that it is farthest away from the oxygen vacancies,[8] i.e., there exist multiple configurations for $4f$ electrons to locate at various neighboring Ce ions (at the first-, second-, third-, and fourth-neighbor positions next to the vacancy).[9] It is also recently revealed both by the DFT+U calculations[10] and scanning tunneling microscopy (STM)[11,12] that the vacancy is bound to the Ce^{4+} ions, whereas Ce^{3+} ions occupy more distant coordination shells.

Contrary to these studies, Castleton *et al.*[13] have shown that the localization of electrons at the Ce $4f$ level is very incomplete. It reaches a maximum at about 80% of the Ce $4f$ charge for $U \sim 6$ eV, and for higher U it decreases rapidly as charge is transferred onto second-neighbor O ions and beyond. Recently, Han *et al.*[14] have shown that with increasing oxygen deficiency, the electrons left behind after the oxygen removal not only localize on Ce $4f$ orbitals but also on the vacancy sites. In all these studies the source of controversy is not the existence of Ce^{3+} ions, which is confirmed in many experimental studies,[15,16] but the degree of localization of electrons at the f level of the Ce^{3+} ions. The question then is, do electrons transfer onto neighboring O ions or vacancies when the oxygen deficiency becomes large?

In this paper, using Raman scattering measurements on $Ce_{1-x}Fe_x^{2+(3+)}O_{2-y}$ ($x = 0$, 0.06, and 0.12) nanocrystals we show that Ce $4f$ spin electrons are partially delocalized from Ce ions on the Ce(Fe)-O $2p$(V_O)-Ce(Fe) orbitals. Delocalization of electrons causes Raman mode softening, asymmetry, and broadening through the electron-molecular vibration (e-mv) coupling. We have evaluated e-mv coupling using Allen's formula[17] and determined the F_{2g} mode electron-phonon coupling constant λ for pure and Fe-doped nanocrystalline samples. The density of electron state at the Fermi level per spin and molecule $N(0) = 22$ 1/eV was obtained from the linear slope of linewidth (γ) vs frequency shift ($\Delta\omega$) dependence. Delocalization of electrons from Ce^{3+} ions leads to the insulator-to-metal transition in highly oxygen-deficient nanoceria, which is confirmed by the far-infrared reflectivity measurements. New insight into the electronic band structure of defective nanocrystalline ceria is also presented.

II. EXPERIMENTAL

The self-propagating room-temperature synthesis method was used to produce pure and Fe-doped nanocrystals of high quality with a narrow size particle distribution in the nanometric range. Starting materials were metal nitrates and sodium hydroxide. The details of the sample preparation procedure can be found in our recent publications.[18,19] Micro-Raman spectra were taken in backscattering configuration and analyzed using a Jobin Yvon T64000 spectrometer equipped with a nitrogen-cooled charge-coupled-device detector. As an excitation source we used the 647.1-nm, 514.5-nm, and 488- nm lines of a Coherent Innova 70C spectrum Ar/Kr mixed gas-ion laser with an average power less than 10 mW to avoid sample heating. Far-infrared reflectivity spectra were measured at room temperature using a Bomem DA-8 Fourier transform spectrometer. Photoluminescence spectra were measured at room temperature using a Jobin Yvon U1000

monochromator equipped with an RCA31034A photomultiplier as a detector. The excitation source was the 442-nm line of a He-Cd laser.

III. RESULTS AND DISCUSSION

Cerium oxide crystalizes in the fluorite-type cubic crystal structure [see Fig. 1(c)], the space group $Fm\bar{3}m$ (no. 225), in which Ce is located in 4*a* position (0;0;0), surrounded by eight O located at 8*c* position ($\frac{1}{4};\frac{1}{4};\frac{1}{4}$). This structure has one Raman active triply degenerate F_{2g} mode, which in polycrystalline and single-crystal samples appears at about 465 cm^{-1}.[20] This mode represents stretching vibrations of only oxygen atoms around Ce. In our less than 5 nm CeO_{2-y} nanocrystals[2] this mode is centered at about 457 cm^{-1} [Fig. 1(a), 1(b)], exhibiting strong red shift and asymmetrical broadening regarding the bulk counterpart.[21,22] Beside the main F_{2g} band appears an additional structure at about 600 cm^{-1} in the Raman spectra of ceria nanocrystals. This structure is assigned to the oxygen-vacancy-related Raman active mode[20,23] because of the nonstoichiometry of nanosamples.

Several factors such as phonon confinement, strain, nonhomogeneity of the size distribution, defects, and variations in phonon relaxation with particle size can contribute to the changes in the Raman peak position and linewidth of the F_{2g} mode. In a nanocrystal the phonons are confined in space, and all the phonons over the entire Brillouin zone will contribute to the first-order Raman spectra. The weight of the off-center phonons increases as the crystal size decreases, and the phonon dispersion causes an asymmetrical broadening and the frequency shift of the Raman mode. The influence of all these effects on the Raman mode intensity, shape, and energy was recently discussed in Ref. 24.

On the other hand, Raman mode softening and broadening can appear as a consequence of the electron-molecular vibration (phonon) coupling.[25] As we discussed in the case of Na and Ca vanadates,[26,27] the force constant of the Raman mode at 448 cm^{-1} in α'-NaV_2O_5 (which represents vibration of oxygen ions) is strongly affected by the electron charge (which is delocalized on V-O-V orbitals). Because of that, this mode appears at a frequency below its intrinsic value of 485 cm^{-1} in pure V_2O_5 or 470 cm^{-1} in CaV_2O_5 (where spin electrons are attached to the V^{4+} ions).[27] In addition, this mode in α'-NaV_2O_5 shows pronounced asymmetry and broadening. Accordingly, we can consider the observed asymmetry and broadening of the F_{2g} Raman mode in our CeO_{2-y} nanocrystalline sample in part as charge effect related if electrons are transferred from the Ce $4f^1$ level into O $2p$ (or vacant V_O) sites [Ce $4f$-O $2p(V_O)$-Ce $4f$ bonds].

The oxygen vacancy distribution and charge effects on the Raman spectra of nanocrystalline CeO_{2-y} can be studied:

(i) by measuring the Raman spectra on CeO_{2-y} nanocrystals with various incident laser excitation lines or

(ii) by measuring the Raman spectra of CeO_{2-y} nanocrystals doped with the same dopant concentration (in our case Fe) in a different valence state.

In the first case, because of higher vacancy concentration followed by an accumulation of charge more in the surface layers than in the inner part of the CeO_{2-y} nanocrystalline sample,[28] we are expecting to observe changes in the Raman spectra using various excitation energies. In fact, the laser light penetration depth depends on the incident light wavelength and absorption coefficient of the sample. The higher the energy, the smaller the penetration depth, providing information about surface properties rather than properties of the inner part of the nanocrystal. Therefore the observable difference in the Raman spectra measured with various excitation lines should be charge effect related.

Figure 2 shows the Raman spectra of $Ce_{0.88}Fe^{2+}_{0.12}(Fe^{3+}_{0.12})O_{2-y}$ samples measured with various excitation energies. As we expected, the largest F_{2g} mode broadening in the $Fe^{2+(3+)}$- doped samples is manifested at the highest excitation energy (488-nm line), due to higher oxygen deficiency and charge accumulation on the nanoparticle surface. Having in mind the ability of CeO_{2-y} to release oxygen easily, we have also demonstrated that keeping the ceria sample in vacuum leads to a dramatic increase of oxygen

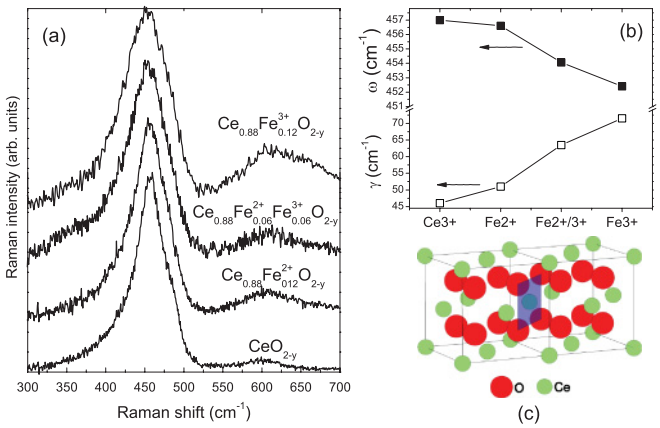

FIG. 1. (Color online) (a) Raman spectra of $Ce_{1-x}Fe_x{}^{2+(3+)}O_{2-y}$ ($x = 0$, 0.06, and 0.12) 5 nm-sized nanocrystals measured at room temperature using $\lambda_L = 514.5$ nm excitation. (b) Raman mode linewidth and frequency change in the samples from Fig. 1(a). (c) Schematic representation of CeO_2 crystal structure.

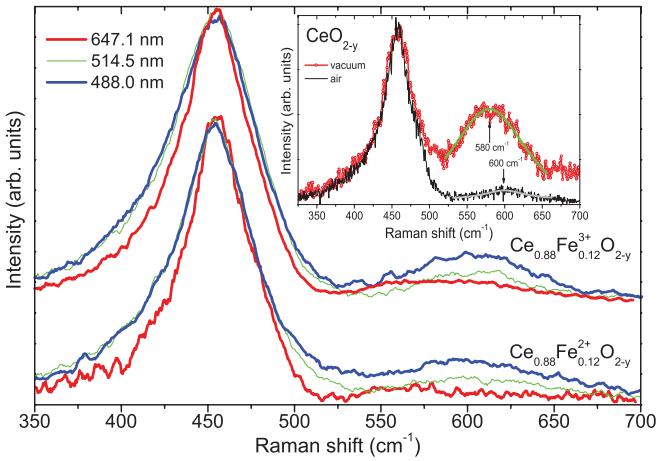

FIG. 2. (Color online) Room-temperature Raman spectra of $Ce_{0.88}Fe_{0.12}{}^{2+(3+)}O_{2-y}$ nanocrystals measured using various excitation energies. Inset: Raman spectra of a CeO_{2-y} nanocrystalline sample measured at room temperature in air and under vacuum of 10^{-4} Torr using $\lambda_L = 514.5$ nm excitation.

deficiency and charge accumulation at the sample surface. In the inset of Fig. 2 is shown how the vacuum treatment at room temperature caused further F_{2g} Raman mode broadening, whereas the intrinsic vacancy-related mode at about 600 cm^{-1} changes its energy (softens for about 20 cm^{-1}) and broadens significantly (the FWHM changes from 64 to 134 cm^{-1}).

In the second case, different valence states of dopant allow study of the influence of charge on the Raman spectra in the CeO_{2-y} samples. Among all 3*d* elements only iron (and cobalt[29]) can coexist in CeO_2 both in 2+ or 3+ valence state (depending on the preparation procedure[18,19]). Iron in 2+ and/or 3+ valence states can be in low ($\uparrow\downarrow\uparrow\downarrow\uparrow\downarrow$, S = 0 for Fe^{2+} or $\uparrow\downarrow\uparrow\downarrow\uparrow$, S = 1/2 for Fe^{3+}) or high ($\uparrow\downarrow\uparrow\uparrow\uparrow\uparrow$, S = 2 for Fe^{2+} or $\uparrow\uparrow\uparrow\uparrow\uparrow$, S = 5/2 for Fe^{3+}) spin state in an octahedral surrounding by oxygen ions, only in high spin states for a tetragonal oxygen surrounding, and only in low spin states for a square planar surrounding. Because Ce(Fe) ions are located in the center of the oxygen cube, the Ce(Fe) surrounding is nearly square planar [shaded plane in Fig. 1(c)]. Consequently, in investigated samples, $Fe^{2+(3+)}$ ions can be in low spin state only. This fact is experimentally proved by Mössbauer spectroscopy measurements on these samples,[2] which revealed that both $Fe^{2+/3+}$ ions are in paramagnetic, low spin states.

In the Fe^{2+}-doped sample divalent iron in the low spin ($S = 0$) state, which entered substitutionally into the ceria lattice, has no unpaired electrons and we do not expect additional charge influence on the F_{2g} Raman mode. The small change of F_{2g} mode energy in Fe^{2+}-doped ceria compared with undoped ceria is a consequence of oxygen vacancy concentration increase by doping with divalent ions. By doping of ceria with the Fe^{3+} ions an extra electron is provided, which can be transferred to the oxygen or the oxygen vacancy density of states, influencing at the same time the force constants of the corresponding CeO_2 Raman mode.

Figure 3 shows room-temperature Raman spectra of CeO_2 polycrystals, undoped CeO_{2-y} nanocrystals of various sizes, and Fe-doped $Ce_{1-x}Fe_x^{2+}(Fe^{3+})_xO_{2-y}$ ($x = 0$, 0.06, and 0.12) nanocrystals. As seen from Fig. 3, reduction of nanocrystal size produces the F_{2g} mode softening, line broadening, and a pronounced line asymmetry characteristic for very fine, nonstoichiometric nanocrystals. The most pronounced softening and broadening of the F_{2g} Raman mode is clearly observed in the $Fe^{2+/3+}$-doped samples [Fig. 1(b)]. At first glance, such behavior of the F_{2g} Raman mode was unexpected if we have in mind a change of the CeO_2 unit cell parameter with Fe doping, only. In fact, the doping of ceria with ions of smaller ionic radius such as $Fe^{2+(3+)}$ ions causes shrinkage of the unit cell[19] and consequently will contribute to the shift of the F_{2g} mode to higher energies, i.e., mode hardening. Besides that, the x-ray diffraction results[19] showed also that undoped and Fe-doped samples have similar crystallite size ($\leqslant$5 nm), leading to the conclusion that confinement effects cannot be responsible for the additional broadening and softening of the F_{2g} mode in Fe-doped samples.

Ce $4f^1$ electrons, which are localized on the Ce^{3+} ions, have no influence on the Raman spectra. Only delocalized $4f$ electrons, located at Ce(Fe)-O(V_O)-Ce(Fe) orbitals, can modulate force constants of the corresponding Raman modes, resulting in Raman mode softening and asymmetry. Since

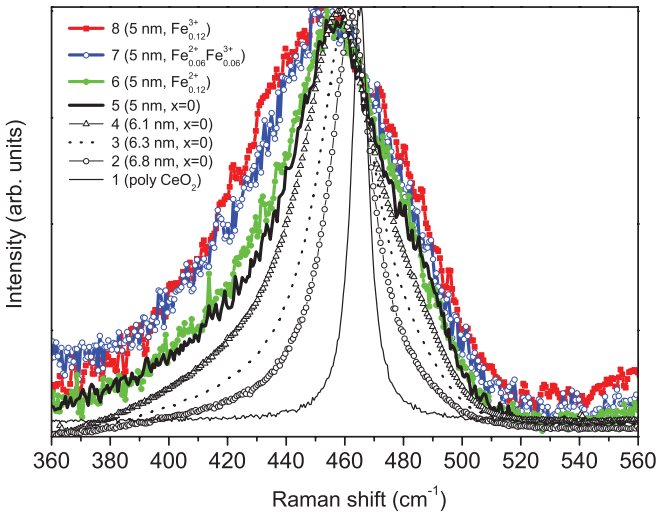

FIG. 3. (Color online) Raman spectra of polycrystalline CeO_2 and $Ce_{1-x}Fe_x^{2+(3+)}O_{2-y}$ ($x = 0$, 0.06, and 0.12) nanocrystals measured at room temperature using $\lambda_L = 514.5$ nm. The sizes of nanocrystals, obtained from x-ray diffraction (Raman) techniques, are: 3 (5) nm (samples 5–8); 4.1 (6.1) nm–sample 4; 4.5 (6.3) nm–sample 3; 5.7 (6.8) nm–sample 2.

there is evident asymmetry, softening, and broadening of both the F_{2g} and the intrinsic vacancy modes, we point out that the $4f$ electrons are partially delocalized onto the Ce(Fe)-O(V_O)-Ce(Fe) orbitals. Therefore the observed softening and broadening of the F_{2g} mode (Figs. 1 and 3) in $Fe^{2+/3+}$-doped samples are not size but charge effect related, and can be only a consequence of the electron-molecular vibration coupling. According to the Raman spectra, it can be concluded that it is energetically favorable for a d^5 electron of Fe^{3+} ion to be transferred to the oxygen or oxygen vacancy density of states than to be localized on the Fe ion.

For a description of the relation between phonon linewidth and e-mv coupling constants for single-particle excitation, Allen's formula[17] can be used,

$$\gamma_i = \frac{1}{g_i}\frac{\pi}{2}N(0)\lambda_i\omega_{bi}^2, \qquad (1)$$

where for each of the modes the γ_i is the FWHM of the line, $N(0)$ is the density of states at the Fermi level per spin and molecule, λ_i the dimensionless electron-phonon coupling constants, g_i the mode degeneracy, and ω_{bi} is the bare phonon frequency (uncoupled to the charge). Allen's formula has been successfully used for the evaluation of Raman mode softening due to electron-molecular vibration (phonon) coupling in many other systems.[30,31]

Within the framework of Allen's theory there should be a linear relation between linewidth and the difference between the bare phonon frequency and the observed frequency $\Delta\omega$. This relation can be expressed in the form[30]

$$\gamma = -\frac{\pi}{2}N(0)\omega_b\Delta\omega. \qquad (2)$$

Experimentally obtained values of the Raman mode linewidth γ vs $\Delta\omega$ [Fig. 1(b)] are plotted in Fig. 4. The F_{2g} mode value of 465 cm^{-1} of the polycrystalline sample is used for the bare phonon frequency. First, we consider the

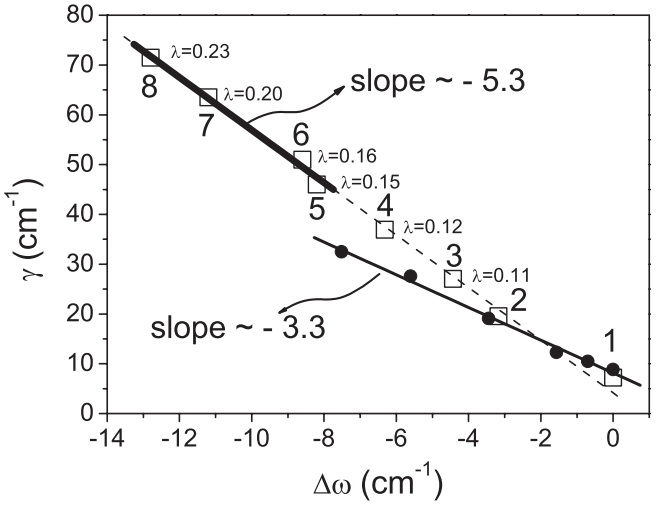

FIG. 4. Plot of linewidth γ versus frequency shift $\Delta\omega$ of F_{2g} Raman mode in undoped (2–5) and Fe-doped (6–8) samples. Solid circles are data from Ref. 35.

γ vs $\Delta\omega$ dependance for undoped and Fe-doped samples of the nearly the same nanocrystal size (5 nm), denoted with numbers, 5, 6, 7, and 8 in Fig. 4. Linear fit of the γ vs $\Delta\omega$ dependence is in agreement with Eq. (2) and supports our assumption to use Allen's model. It is worth mentioning that other nanocrystalline samples follow the same linear γ vs $\Delta\omega$ dependence (at least samples 3 and 4, see Fig. 4). Although these nanocrystalline samples have slightly greater grain sizes, they are highly oxygen deficient, demonstrating that charge-induced line broadening is higher that other line-broadening effects (grain size or strain effects[24]).

Before determining of the density of states $N(0)$ and e-mv coupling constant λ from Allen's formula [Eqs. (1) and (2)], we should first consider the electronic structure of nanoceria in detail. The CeO_2 is an insulator in a crystalline phase with energy gap between the valence band (formed from O $2p$ states) and upper conduction band (formed of Ce $5d$ states) of about 6 eV [Fig. 5(a)]. Inside the gap there is a lower conduction band composed of Ce $4f^0$ states. This band is about 4 eV away from the top of the valence band.[6] Due to nonstoichiometry, i.e., an appearance of oxygen vacancies and consequently Ce^{3+} ions, the electronic structure of cerium oxide changes drastically. In fact, the empty $4f^0$ lower conduction band splits into two $4f$ energy bands: the lower Ce $4f^1$ (occupied) and upper Ce $4f^0$ (empty) band. The existence of these bands inside the energy gap of nonstoichiometric ceria was recently confirmed by STM measurements.[11,12] The Ce $4f^1$ (occupied) band is at about 0.9 eV, and the Ce $4f^0$ (empty) band is at about 4.4 eV away from the top of the valence band[11] [see Fig. 5(b)]. It is also revealed[11,12] that the position of the $4f^1$ occupied band moves toward the valence band as the Ce^{3+}/Ce^{4+} ions occupy different positions around the oxygen vacancy.

In nanoceria, the oxygen deficiency is further increased, which leads to additional increase of Ce^{3+} ion concentration. Due to electron delocalization into Ce $4f$-O $2p$-Ce $4f$ orbitals ($f-p$ hybridization), electrons from Ce^{3+} ions move to the oxygen O $2p$ states in the valence band.[32] This transition is associated with overlapping of $4f^1$ and valence band density of states [Fig. 5(c)].

From the other side, randomly distributed structural defects in CeO_2 (oxygen and ceria vacancies), as in any other semiconductor, lead to the formation of localized states within the forbidden gap. In heavily doped semiconductors (in our case highly oxygen-deficient nanoceria), the defect-related energy levels merge to form a narrow energy band known as an "impurity band" or "defect-related band." At higher concentration, when the defects (impurities) are close enough, quantum overlapping of electron wave functions tends to delocalize them, leading to a metallic behavior with a Fermi level pinned inside the impurity band[33] [see Fig. 5(c)]. Charge carrier energies now lie near the edge but within the band of delocalized states because of overlapping with $4f^1$ and valence band states. The existence of a very narrow (200-meV) defect-related band within the CeO_2 energy gap was recently observed using STM spectroscopy[11] also.

In order to check this scenario of the insulator-to-metal transition in nanoceria by an increase of oxygen deficiency, two additional spectroscopic techniques were applied: the far-infrared reflectivity measurements and photoluminescence. A room-temperature far-infrared reflectivity spectrum of a nanoceria sample [Fig. 5(d)] is compared to the reflectivity spectrum of single-crystal CeO_2 (Ref. 34). As can be seen from Fig. 5(d), the phonon structure between 270 (TO mode) and 570 cm^{-1} (LO mode) is screened in the nanoceria sample with an electronic background of metallic origin (reflectivity due to photon scattering on free charge carriers), which is in the low-frequency region well fitted with the Hagen-Rubens

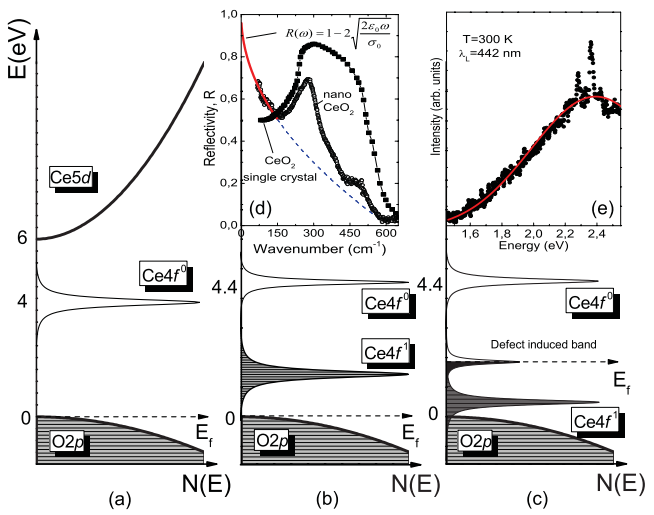

FIG. 5. (Color online) Schematic representation of the evolution of the electronic density of states and band structure of cerium oxide with increasing oxygen deficiency: (a) stoichiometric sample, (b) nonstoichiometric sample, (c) nano-CeO_2, and (d) far-infrared reflectivity spectra of single-crystal[34] and nanoceria. The solid line in low-frequency region represents metallic contribution to the reflectivity spectrum calculated using the Hugen-Rubens formula for metals. (e) Room-temperature photoluminescence spectrum of the CeO_2 nanocrystalline sample (circles) together with a Gaussian line profile fit (solid line).

approximation, commonly used for frequency dependence of reflectivity in metals [solid line in Fig. 5(d)].

The room-temperature photoluminescence spectrum of the same sample is given in Fig. 5(e). The excitation energy was 2.8 eV (the 442-nm line of a He-Cd laser). This energy is enough to excite (inside of the gap) only electron transitions between the defect-related band and the lower ($4f^0$) conduction band. (The energy difference between the $4f^0$ and $4f^1$ bands is about 3.5 eV.[11]) According to the photoluminescence spectrum from Fig. 5(e), there is a peak structure at about 2.4 eV which can represent recombination of the photo-excited carriers from the $4f^0$ level to the defect-related band. This value is in accordance with STM results.[11] Having all the above-mentioned in mind, all necessary conditions (metallic state with the defect-related narrow energy band with the Fermi level pinned inside of this band) for application of the Allen's formula are satisfied.

We now refer back to Fig. 4 where γ (FWHM) vs $\Delta\omega$ dependence is shown. According to Eq. (2), the slope of this linear function ($y = A + Bx$) can be used for determination of the density of states at the Fermi level per spin and molecule $N(0)$. The total slope of $B = -5.3$ (± 0.25) (Fig. 4) of the $\gamma = f(\Delta\omega)$ dependence can be divided into two components: B_1, which represents the mode-broadening increase influenced by charge, and B_2, which represents mode broadening due to the size effects (crystallite size and strain). In order to distinguish these two mode-broadening contributions, we have used size-effect-related dependencies of the peak position and linewidth of the F_{2g} mode in pure nanoceria given by Spanier *et al.* in Fig. 6 of Ref. 35. In fact, for each sample, whose $1/x$ values (x= particle size in nanometers) are given in Fig. 6: 0 (polycrystalline sample), 0.04 (25 nm), 0.067 (15 nm), 0.1 (10 nm), 0.135 (7.4 nm), and 0.164 (6.1 nm), we took experimental data of the peak position [Fig. 6(a)] and linewidth [Fig. 6(b)] [denoted by crosses (X) in Fig. 6]. Using these values we have drawn the linewidth γ vs $\Delta\omega$ dependence ($\omega_0 = 464.4\ \mathrm{cm}^{-1}$), shown by solid circles in Fig. 4. A linear fit of these data gives a slope of -3.3 (± 0.25). Thus pure charge contribution to the linear slope becomes $B_1 = B - B_2 = -2$ (± 0.5). For this slope value we have estimated the value of the density of states of the defect-related band at the Fermi level per spin and molecule of $N(0) = 22\ (\mathrm{eV})^{-1}$. A relatively high density of states value, which is a consequence of colossal change of Raman mode linewidth in nano CeO_{2-y}, is within the range of reported values.[30]

Finally, Eq. (1) allows calculation of the e-mv coupling constant λ for undoped and Fe-doped samples. In the case of CeO_{2-y} F_{2g} mode [$g = 3$, $N(0) = 22\ (\mathrm{eV})^{-1}$, and $\omega_b = 465\ \mathrm{cm}^{-1}$] we obtained $\lambda = 0.15$. In the Fe-doped samples λ increases (see Fig. 4) and reaches the value $\lambda = 0.23$ for the $Fe^{3+}_{0.12}$ -doped sample. The increasing trend of λ is in complete accordance with F_{2g} Raman mode behavior, implying that the strongest e-mv coupling is in the $Fe^{3+}_{0.12}$-doped sample.

In conclusion, we reported the Raman study of pure and iron-doped $Ce_{1-x}Fe_x^{2+(3+)}O_{2-y}$ ($x = 0$, 0.06, and 0.12) nanocrystals. The Raman F_{2g} mode exhibits unexpected softening and broadening by changing the valence state of dopant as a consequence of electron-molecular vibrations coupling. This finding supports an assumption that electrons in highly oxygen-deficient pure and Fe-doped ceria samples are not only attached at Ce^{3+} ions but also delocalized onto Ce(Fe)-O(V_O)-Ce(Fe) orbitals. Delocalization of electrons from Ce^{3+} ions is followed with the insulator-to-metal transition in highly oxygen-deficient nanoceria, which was confirmed by measuring the far-infrared reflectivity. The electron-molecular vibration coupling constant λ for F_{2g} mode in pure and Fe-doped samples and density of electron states of the defect-based band at the Fermi level per spin and molecule $N(0) = 22\ (\mathrm{eV})^{-1}$ were determined within the framework of Allen's theory. Finally, these findings provided new insight into the electronic band structure of defective nanoceria presented in this work.

ACKNOWLEDGMENTS

This work was financially supported by the Serbian Ministry of Education and Science under Projects No. ON171032, No. III45018, and No. SCOPES IZ730-128169. We thank Branko Matovic for the samples and S. Aškrabić for the photoluminescence measurements.

[1] A. Sundaresan and C. N. R. Rao, Nanotoday **4**, 94 (2009).
[2] Z. D. Dohčević-Mitrović, N. Paunović, M. Radović, Z. V. Popović, B. Matović, B. Cekić, and V. Ivanovski, Appl. Phys. Lett. **96**, 203104 (2010).
[3] N. V. Skorodumova, R. Ahuja, S. I. Simak, I. A. Abrikosov, B. Johansson, and B. I. Lundqvist, Phys. Rev. B **64**, 115108 (2001).
[4] J. L. F. Da Silva, M. V. Ganduglia-Pirovano, J. Sauer, V. Bayer, and G. Kresse, Phys. Rev. B **75**, 045121 (2007).
[5] D. A. Andersson, S. I. Simak, B. Johansson, I. A. Abrikosov, and N. V. Skorodumova, Phys. Rev. B **75**, 035109 (2007).
[6] N. V. Skorodumova, S. I. Simak, B. I. Lundqvist, I. A. Abrikosov, and B. Johansson, Phys. Rev. Lett. **89**, 166601 (2002).
[7] P. R. L. Keating, D. O. Scanlon, and G. W. Watson, J. Phys.: Condens. Matter **21**, 405502 (2009).
[8] E. Shoko, M. F. Smith, and R. H. McKenzie, J. Phys.: Condens. Matter **22**, 223201 (2010).
[9] H. Y. Li, H. F. Wang, X. Q. Gong, Y. L. Guo, Y. Guo, G. Lu, and P. Hu, Phys. Rev. B **79**, 193401 (2009).
[10] M. V. Ganduglia-Pirovano, J. L. F. Da Silva, and J. Sauer, Phys. Rev. Lett. **102**, 026101 (2009).
[11] X. Shao, J. F. Jerratch, N. Nilius, and H. J. Freund, Phys. Chem. Chem. Phys. **13**, 12646 (2011).
[12] J. F. Jerratsch, X. Shao, N. Nilius, H. J. Freund, C. Popa, M. V. Ganduglia-Pirovano, A. M. Burow, and J. Sauer, Phys. Rev. Lett. **106**, 246801 (2011).
[13] W. M. Castleton, J. Kullgren, and K. Hermansson, J. Chem. Phys. **127**, 244704 (2007).
[14] X. Han, J. Lee, and H. I. Yoo, Phys. Rev. B **79**, 100403(R) (2009).
[15] L. R. Shah, B. Ali, H. Zhu, W. G. Wang, Y. Q. Song, H. W. Zhang, S. I. Shah, and J. Q. Xiao, J. Phys.: Condens. Matter **21**, 486004 (2009).

[16]V. Fernandes, P. Schio, A. J. A. de Oliveira, W. A. Ortiz, P. Fichtner, L. Amaral, I. L. Graff, J. Varalda, N. Mattoso, W. H. Schreiner, and D. H. Mosca, J. Phys.: Condens. Matter **22**, 216004 (2010).
[17]P. B. Allen, Solid State Commun. **14**, 937 (1974).
[18]M. Radović, Z. Dohčević-Mitrović, N. Paunović, M. Šćepanović, B. Matović, and Z. V. Popović, Acta Phys. Pol. A **116**, 84 (2009), http://przyrbwn.icm.edu.pl/APP/PDF/116/a116z119.pdf
[19]B. Matović, Z. Dohčević-Mitrović, M. Radović, Z. Branković, G. Branković, S. Bošković, and Z. V. Popović, J. Power Sources **193**, 146 (2009).
[20]W. H. Weber, K. C. Hass, and J. R. McBride, Phys. Rev. B **48**, 178 (1993).
[21]Z. V. Popović, Z. Dohčević-Mitrović, A. Cros, and A. Cantarero, J. Phys. Condens. Matter **19**, 496209 (2007).
[22]Z. D. Dohčević-Mitrović, M. Šćepanović, M. U. Grujić-Brojčin, Z. V. Popović, S. B. Bošković, B. M. Matović, M. V. Zinkevich, and F. Aldinger, Solid State Commun. **137**, 387 (2006).
[23]A. Nakajima, A. Yoshihara, and M. Ishigame, Phys. Rev. B **50**, 13297 (1994).
[24]Z. V. Popović, Z. D. Dohčević-Mitrović, M. Šćepanović, M. U. Grujić-Brojčin, and S. Aškrabić, Ann. Phys. (Berlin) **523**, 62 (2011).
[25]Z. V. Popović, V. A. Ivanov, O. P. Khoung, T. Nakamura, G. Saito, and V. V. Moshchalkov, Synth. Met. **124**, 421 (2001).
[26]Z. V. Popović, M. J. Konstantinović, R. Gajić, V. N. Popov, M. Isobe, Y. Ueda, and V. V. Moshchalkov, Phys. Rev. B **65**, 184303 (2002).
[27]Z. V. Popović, M. J. Konstantinović, V. V. Moshchalkov, M. Isobe, and Y. Ueda, J. Phys.: Condens. Matter **15**, L139 (2003).
[28]J. M. D. Coey, K. Wongsaprom, J. Alaria, and M. Venkatesan, J. Phys. D: Appl. Phys. **41**, 134012 (2008); J. M. D. Coey, P. Stamenov, R. D. Gunning, M. Venkatesan, and K. Paul, New J. Phys. **12**, 050325 (2010).
[29]V. Fernandes, J. J. Klein, N. Mattoso, D. H. Mosca, E. Silveira, E. Ribeiro, W. H. Schreiner, J. Varalda, and A. J. A. de Oliveira, Phys. Rev. B **75**, 121304 (2007).
[30]J. Winter and H. Kuzmany, Phys. Rev. B **53**, 655 (1996).
[31]A. Graja, R. Lipiec, and M. Polomska, J. Mol. Struct. **555**, 131 (2000).
[32]R. Fors, S. I. Khartsev, and A. M. Grishin, Phys. Rev. B **71**, 045305 (2005).
[33]X. Blase, E. Bustarret, C. Chapelier, T. Klein, and C. Marcenat, Nature Mater. **8**, 375 (2009).
[34]F. Marabelli and P. Wachter, Phys. Rev. B **36**, 1238 (1987).
[35]J. E. Spanier, R. D. Robinson, F. Zhang, S. W. Chan, and I. P. Herman, Phys. Rev. B **64**, 245407 (2001).